9 September 2002

ELSEVIER

Chemical Physics Letters 363 (2002) 372–380

CHEMICAL PHYSICS LETTERS

www.elsevier.com/locate/cplett

# Creating isotropic dipolar spectra for a pair of dipole coupled spins in high-field

Jamie D. Walls, Wyndham B. Blanton, Robert H. Havlin, Alexander Pines *

*Department of Chemistry, Materials Sciences Division, Lawrence Berkeley National Laboratory, University of California, MC 1460, Berkeley, CA 94720-1460, USA*

Received 20 May 2002; in final form 19 July 2002

**Abstract**

In the absence of a strong magnetic field, the dipolar interaction between two nuclear spins is independent of orientation leading to sharp lines. However, in high magnetic fields the Zeeman interaction breaks the symmetry of space and spin producing an anisotropic dipolar spectra. In the following Letter, a method that yields isotropic dipolar spectra for a pair of dipole-coupled spins is presented. This is accomplished through a suitable choice of coherence pathways and average Hamiltonians. We present a theoretical explanation as well as an experimental verification for this novel methodology. © 2002 Elsevier Science B.V. All rights reserved.

## 1. Introduction

Nuclear magnetic resonance (NMR) can provide a wealth of information about the structure of molecules. In particular, liquid state NMR has been able to help determine the structures of molecules of up to $\approx 110$ kD with the size limits being continually increased [1]. However, many interesting systems, such as the prion protein [2,3], silk [4], zeolites [5], etc., are not amenable to liquid state studies and must be examined in the solid state. Certain interactions such as dipole–dipole couplings and/or chemical shift anisotropy (CSA), normally averaged away by molecular motion in liquids, are present in solids and affect the NMR spectra significantly. These interactions are sensitive to molecular structure and have been demonstrated to be very useful in the assignment of structure in molecules. In particular, dipole–dipole couplings, due to their dependence upon the distance between the interacting spins, have been useful in placing structural constraints on molecules in solids [6].

In zero magnetic field, the dipolar Hamiltonian for a pair of spins is given by

$$H_{\mathrm{D}}^{\mathrm{ZF}} = \omega_{\mathrm{D}}(\overrightarrow{I^1}\cdot\overrightarrow{I^2} - 3(\overrightarrow{I^1}\cdot\hat{\boldsymbol{r}}_{12})(\overrightarrow{I^2}\cdot\hat{\boldsymbol{r}}_{12})) = \omega_{\mathrm{D}}\sum_{m=-2}^{2}(-1)^m A_{2,m}^{12}(\theta_{12},\phi_{12})T_{2,-m}^{12}, \quad (1)$$

where $\hat{\boldsymbol{r}}_{12}$ is the internuclear unit vector between spins 1 and 2, $\omega_{\mathrm{D}} = (\gamma_1\gamma_2)/|r_{12}|^3$ is the dipole coupling, $A_{2,m}^{12}(\theta_{12},\phi_{12})$ and $T_{2,m}^{12}$ are second rank spatial and spin tensors respectively, and $(\theta_{12},\phi_{12})$ are

* Corresponding author. Fax: +1-510-486-5744.
*E-mail address:* pines@cchem.berkeley.edu (A. Pines).

0009-2614/02/$ - see front matter 
PII: S0009-2614(02)01188-0

polar angles relating the magnetic field quantization axis to the internuclear vector. For two spin 1/2 particles, the eigenvalues of $H_{\mathrm{D}}^{\mathrm{ZF}}$ are independent of $\theta_{12}$ and $\phi_{12}$, which for a powdered sample, result in three sharp lines, as shown in Fig. 1a.

Typically, NMR experiments are performed under high magnetic fields for reasons of sensitivity and resolution. However, the Zeeman interaction, $H_{\mathrm{Zeeman}} = \gamma \overrightarrow{B_0} \cdot \vec{I}$, destroys the isotropy of spin and space. In high magnetic fields, where $|\gamma B_0| \gg |\omega_{\mathrm{D}}|$, the dipolar interaction is treated as a perturbation to the Zeeman interaction, causing $H_{\mathrm{D}}^{\mathrm{ZF}}$ in Eq. (2) to be effectively truncated along the Zeeman field. Taking the magnetic field, $\overrightarrow{B_0}$ to be along the $z$ axis, the 'secular' part of the dipolar Hamiltonian, $H_{\mathrm{D}}^{\mathrm{HF}}$, is given by

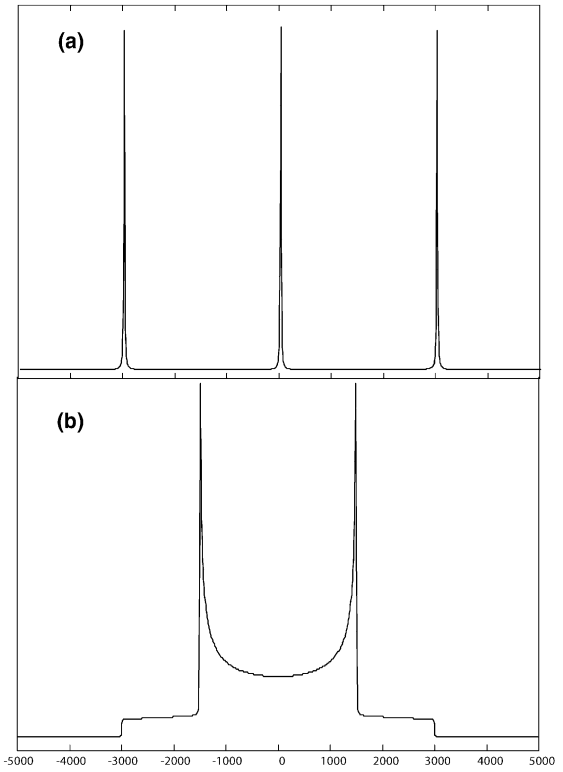


Fig. 1. Simulated spectra for a dipole coupled spin system in (a) zero-field and (b) high-field conditions. An $\omega_{\mathrm{D}}/(2\pi) = 2000$ Hz was used. (a) The zero-field consists of three sharp lines at frequencies at 0 Hz and ±3000 Hz. (b) Pake pattern for a dipole coupled spin system, where the spread in frequencies is due to the anisotropy of $H_{\mathrm{D}}^{\mathrm{HF}}$ in Eq. (2).

$$H_{\mathrm{D}}^{\mathrm{HF}} = \omega_{\mathrm{D}} A_{2,0}^{12}(\theta_L, \phi_L) T_{2,0}^{12} = \omega_{\mathrm{D}} \frac{3\cos^2(\theta_L) - 1}{2} \left( 3I_Z^1 I_Z^2 - \overrightarrow{I^1} \cdot \overrightarrow{I^2} \right). \quad (2)$$

The eigenvalues of $H_{\mathrm{D}}^{\mathrm{HF}}$ depend upon $\theta_L$, the angle that the internuclear vector $\vec{r}_{12}$ makes with the Zeeman field. For a powdered sample, this results in a broad spectrum with the typical Pake pattern for a pair of homonuclear dipole coupled spins (Fig. 1b). This anisotropic broadening limits resolution and complicates spectral assignments of dipolar couplings relative to the isotropic zero-field dipolar spectrum. The first experimental attempts to capitalize on the benefits of evolution in both zero-field and high-field were the shuttling experiments of Weitekamp et al. [7]. In these experiments, the spins were polarized under high-field conditions and then physically removed from the magnet into zero-field conditions. The spins then evolved under $H_{\mathrm{D}}^{\mathrm{ZF}}$ in the indirect dimension and were returned to high-field for direct detection. Subsequently it was realized by Tycko [8–10] that $H_{\mathrm{D}}^{\mathrm{HF}}$, which is the product of two second rank tensors, can be written in a combined space as the sum of zeroth, second, and fourth rank tensors as follows:

$$H_{\mathrm{D}}^{\mathrm{HF}} = \omega_{\mathrm{D}} A_{2,0}^{12} T_{2,0}^{12} = \omega_{\mathrm{D}} \sum_{l=0,2,4} C(2,2,l,0) F_{l,0}, \quad (3)$$

where the $C(2,2,l,0)$ are Clebsch–Gordon coefficients, and $F_{l,0}$ are spherical tensors in the combined space of space and spin. The scalar term $F_{0,0}$ is proportional to the zero-field Hamiltonian, $H_{\mathrm{D}}^{\mathrm{ZF}}$. Through a suitable combination of rotor synchronized pulses, an average Hamiltonian [11], $\overline{H}$, can be created from Eq. (2) that removes the second and fourth rank components leaving

$$\overline{H} \propto F_{0,0} = \sigma H_{\mathrm{D}}^{\mathrm{ZF}}, \quad (4)$$

where $\sigma$ scales the frequencies of $H_{\mathrm{D}}^{\mathrm{ZF}}$ and is dependent on the actual pulse sequence performed with the maximum possible scaling factor being $\sigma_{\max} = 0.2$. Experiments have been successfully performed in the past with values of $\sigma \approx 0.07$–$0.09$ [9,12]. Tycko [10] and Sun and Pines [13] have found optimal solutions to Eq. (4) involving either a DAS-like [14] or DOR-like [15,16] trajectory which give $\sigma = 0.2$. The problem with a DOR-like

solution is that the simultaneous, mechanical rotation about two different axes is difficult experimentally. A DAS-like solution involving two separate rotor axis evolutions suffers from the problem that the Hamiltonians constructed at the different rotor axes typically do not commute. This requires the sample to be switched back and forth between the two axis in order for the average Hamiltonian treatment to be valid, which is also experimentally difficult.

In this Letter an alternative method to Tycko's zero-field in high-field (ZFHF) is given which, for a pair of homonuclear dipole coupled spins, provides isotropic information about the dipole coupling, called homonuclear isotropic evolution (HOMIE). The basic idea utilizes the fact that from Eq. (2) the observed frequencies are proportional to $\omega_{\mathrm{D}}(3\cos^2(\theta)-1)$. If another Hamiltonian is generated with frequencies proportional to $\omega_{\mathrm{D}}\sin^2(\theta)$, the anisotropic contribution to the combined signal is cancelled using the relation $\sin^2(\theta)+\cos^2(\theta)=1$. In this text, the necessary Hamiltonians and pulse sequences used to generate the isotropic dipolar evolutions are given. The methodology is then experimentally verified on a homonuclear dipole spin pair.

## 2. Theory

The general method for obtaining isotropic dipolar spectra is shown in Fig. 2. Consider a pair of homonuclear dipole coupled spins with the initial density matrix, $\rho(0)=I_Z=I_Z^1+I_Z^2$, evolving under the Hamiltonian, $H$, which is given by

$$H=\omega_{\mathrm{D}}h(\theta)\left(3I_X^1I_X^2-\vec{I}^1\cdot\vec{I}^2\right), \tag{5}$$

where $h(\theta)=k((3\cos^2(\theta)-1)/2)$, and $k$ is the scaling factor associated with the particular RF pulse sequence used to generate $H$ from $H_{\mathrm{D}}^{HF}$. After evolution under $H$ for a time $t$, $\rho(t)$ is given by:

$$\begin{aligned}\rho(t)&=\cos\left(\frac{3}{2}\omega_{\mathrm{D}}h(\theta)t\right)I_Z\\&\quad+\mathrm{i}\sin\left(\frac{3}{2}\omega_{\mathrm{D}}h(\theta)t\right)(T_{2,2}-T_{2,-2})\\&=\rho_0(t)+\rho_2(t),\end{aligned} \tag{6}$$

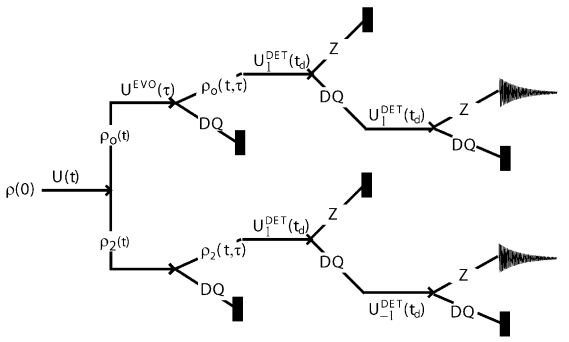


Fig. 2. The Basic procedure in order to obtain isotropic dipolar spectra. An initial density matrix, $\rho(0)=I_Z$ evolves under $H$ (Eq. (5)) to give a $z$-magnetization ($Z$) term, ($\rho_0$), and double-quantum (DQ) term, ($\rho_2$). Both of these terms then evolve under $H^{\mathrm{EVO}}$ (Eq. (7)) and only the $Z$ components are kept. Next, evolution occurs from $Z_0$ and $Z_2$ under $H_1^{\mathrm{DET}}$ into DQ coherence. The DQ coherences are then converted back into $z$-magnetization for detection, using either $H_1^{\mathrm{DET}}$ for the pathway originating from $\rho_0$ or $H_{-1}^{\mathrm{DET}}$ for the pathway originating from $\rho_2$.

where

$$T_{2,\pm2}=I_\pm^1I_\pm^2,\ \rho_0(t)=\cos\left(\frac{3}{2}\omega_{\mathrm{D}}h(\theta)t\right)I_Z,$$

and

$$\rho_2(t)=\mathrm{i}\sin\left(\frac{3}{2}\omega_{\mathrm{D}}h(\theta)t\right)(T_{2,2}-T_{2,-2}).$$

The signal originating from either $\rho_0$ or $\rho_2$ can be distinguished by phase cycling, so in the following the evolution along each pathway will be considered separately.

Consider next the average Hamiltonian, $H^{\mathrm{EVO}}$, of the form

$$H^{\mathrm{EVO}}=\omega_{\mathrm{D}}(gA_{2,-2}T_{2,2}+gA_{2,2}T_{2,-2}), \tag{7}$$

where $A_{2,\pm2}=\frac{3}{4}\sin^2(\theta)\mathrm{e}^{\pm\mathrm{i}2\phi}$, and $g$ is a scaling factor that depends on the particular sequence used to generate $H^{\mathrm{EVO}}$ from $H_{\mathrm{D}}^{\mathrm{HF}}$. The eigenvalues for $H^{\mathrm{EVO}}$ are $\pm\frac{3}{4}g\omega_D\sin^2(\theta)$, which can be used to cancel the anisotropic terms of $h(\theta)$. Evolution of $\rho_0(t)$ under $H^{\mathrm{EVO}}$ for a time $\tau$ gives

$$\begin{aligned}\langle I_Z(t,\tau)\rangle_0&=Tr(\rho_0(t,\tau)I_Z)\\&=\cos\left(\frac{3}{2}\omega_{\mathrm{D}}h(\theta)t\right)\cos(\omega_{\mathrm{D}}w(\theta)\tau),\end{aligned} \tag{8}$$

where $w(\theta)=\frac{3}{2}g\sin^2(\theta)$. Evolution of $\rho_2(t)$ under $H^{\mathrm{EVO}}$ for a time $\tau$ gives

$$\langle I_Z(t,\tau)\rangle_2 = Tr(\rho_2(t,\tau)I_Z) = -\cos(2\phi)\sin\left(\frac{3}{2}\omega_D h(\theta)t\right) \times \sin(\omega_D w(\theta)\tau). \quad (9)$$

The $\theta$ dependence in both Eq. (8) and Eq. (9) involve terms proportional to $\omega_D[h(\theta)t \pm w(\theta)\tau]$ and can be cancelled if

$$\frac{9}{4}kt = \pm\frac{3}{2}g\tau. \quad (10)$$

Neglecting the trivial solution when $k = g = 0$, Eq. (10) implies that at most half of the signal can be made isotropic. Specifically, if the + solution is satisfied from Eq. (10), the frequency terms proportional to $\omega_D[h(\theta)t + w(\theta)\tau]$ will be independent of $\theta$, whereas the frequency terms proportional to $\omega_D[h(\theta)t - w(\theta)\tau]$ will not be independent of $\theta$.

Another difficulty arises due to the $\phi$ dependence of Eq. (9). If the $\cos(2\phi)$ factor were absent from Eq. (9), then Eq. (8) and Eq. (9) could be added or subtracted together to give $\cos(\frac{3}{2}\omega_D h(\theta)t)\cos(\omega_D w(\theta)\tau) \mp \sin(\frac{3}{2}\omega_D h(\theta)t)\sin(\omega_D w(\theta)\tau) = \cos[\omega_D(h(\theta) \pm w(\theta)\tau)]$, thus requiring only one of the equations in Eq. (10) to be satisfied.

The $\phi$ dependence in Eq. (9) can be overcome by evolution under the Hamiltonians, $H_{\pm1}^{DET}$, given by

$$H_{\pm1}^{DET} = \omega_D f(A_{2,\pm1}T_{2,2} - A_{2,\mp1}T_{2,-2}), \quad (11)$$

where $A_{2,\pm1} = \pm\frac{3}{2}\sin(\theta)\cos(\theta)e^{\pm i\phi}$, and $f$ is some scaling factor that is dependent on the particular pulse sequence used to generate $H_{\pm1}^{DET}$ from $H_D^{HF}$. After application of $H_1^{DET}$ for a time $\tau_{DET}$, a double-quantum filter is then applied. For the double-quantum coherences originating from $\rho_0(t,\tau)$, $H_1^{DET}$ is applied for a time $\tau_{DET}$ to convert the double-quantum coherence into $z$-magnetization, giving:

$$\langle I_Z(t,\tau,\tau_{DET})\rangle_0 = -\cos\left(\frac{3}{2}\omega_D h(\theta)t\right) \times \cos(\omega_D w(\theta)\tau) \times \sin^2(\omega_D p(\theta)\tau_{DET}), \quad (12)$$

where $p(\theta) = 3f\sin(\theta)\cos(\theta)$. For the double-quantum coherences originating from $\rho_2(t,\tau)$, $H_{-1}^{DET}$ is applied for a time $\tau_{DET}$ to convert the double-quantum coherence into $z$-magnetization, giving:

$$\langle I_Z(t,\tau,\tau_{DET})\rangle_2 = \sin\left(\frac{3}{2}\omega_D h(\theta)t\right) \times \sin^2(\omega_D w(\theta)\tau)\cos(2\phi) \times \sin^2(\omega_D p(\theta)\tau_{DET}), \quad (13)$$

where $\tau_{DET}$ is fixed for the experiment. Since to lowest order the frequencies in the $t$ and $\tau$ dimensions are independent of $\phi$, the powder average over $\phi$ can be easily performed. For a cylindrically symmetric sample, the signal from Eq. (12) is multiplied by $1/2\pi\int_0^{2\pi} d\phi = 1$ whereas the signal in Eq. (13) is multiplied by $1/2\pi\int_0^{2\pi}\cos^2(2\phi)\,d\phi = 1/2$. The signals originating from $\rho_0$ (Eq. (12)) and $\rho_2$ (Eq. (13)) can then be combined to give

$$S_1 \pm 2S_2 \propto \cos(\omega_D[h(\theta)t \pm w(\theta)\tau]) = C\cos\left[\frac{3}{4}k\omega_D t(3\cos^2(\theta) - 1) \pm \frac{3}{2}\omega_D g\sin^2(\theta)\tau\right], \quad (14)$$

where $t$ and $\tau$ are chosen to satisfy only *one* of the equations in Eq. (10). This gives a scaling factor $\sigma$ of

$$\sigma = \frac{3kt}{2(t+\tau)}. \quad (15)$$

Due to the $H_{DET}$ steps, the total signal is attenuated by the factor $C$ given by

$$C = \frac{1}{3}\left[\frac{1}{2}\int_0^{\pi} d\theta\sin(\theta)\sin^2\left(\frac{3f\omega_D}{2}\sin(2\theta)\tau_{DET}\right)\right] = \frac{1}{6}\left[1 + \sum_{n=0}^{\infty}\frac{J_{2n}(Z)}{16n^2-1}\right], \quad (16)$$

where $Z = 3f\omega_D\tau_{DET}$, and $J_{2n}$ are spherical Bessel functions. The signal intensity is a maximum when $Z \approx 3.8$ with $C \approx 0.24$, and $C \to 1/6$ as $Z \to \infty$.

## 3. Implementation and simulation

In order to generate the different $\theta$-dependencies in the Hamiltonians of Eq. (5), Eq. (7), and

Eq. (11), the sample must be mechanically rotated. Under sample rotation about one axis, the $A_{2,0}$ term in $H_D^{HF}$ (Eq. (2)) becomes time-dependent and is given by

$$\begin{aligned} A_{2,0}(t) &= \frac{1}{2}(3\cos^2(\theta_L(t)) - 1) \\ &= \frac{1}{4}(3\cos^2(\theta) - 1)(3\cos^2(\theta_r) - 1) \\ &\quad + \frac{3}{4}\sin^2(\theta)\sin^2(\theta_r)\sin(2(\omega_r t + \phi)) \\ &\quad + \frac{3}{4}\sin(2\theta)\sin(2\theta_r)\sin((\omega_r t + \phi)), \end{aligned} \quad (17)$$

where $\theta_r$ is the angle that the axis of rotation makes with respect to the magnetic field, $\omega_r$ is the frequency of sample rotation, and $\theta$ and $\phi$ are the polar angles that the internuclear vector makes with respect to the axis of rotation. Since for a pair of spin 1/2 nuclei $[T_{2,0}, T_{2,2}] = [T_{2,0}, T_{2,-2}] = 0$, the addition of a $T_{2,0}$ term into either one of the Hamiltonians, $H^{EVO}$ or $H^{DET}$ from the previous section, will not affect the results given in Eq. (14).

$H^{EVO}$ can be created by a variety of rotor-synchronized RF pulses, each resulting in a different factor, $g$. This factor, $g$, will ultimately limit the achievable scaling factor, $\sigma$, in Eq. (15). A maximal scaling can be achieved by applying $N$ phase-incremented, rotor-synchronized units, with the $k$th unit is given by $[(\pi/2)_0 - \tau_D - (\pi/2)_\pi]_{\phi_k}$, where $\tau_d = 1/(\omega_r N)$ and $\phi_k = 2\pi/N$. Here the pulses are assumed to be $\delta$-pulses. Repeating the sequence with an additional $\pi$ phase shift removes additional terms arising from the CSA and the dipolar interaction to lowest order (e.g., $I_\pm$, $I_Z I_\pm$). Spinning the rotor at an angle $\theta_r$ and applying the above sequence gives

$$g = \frac{3N}{16\pi}\sin\left(\frac{2\pi}{N}\right)\sin^2(\theta_r). \quad (18)$$

To achieve the maximum scaling factor, $\sigma$, consider the following experiment (Fig. 3a): while spinning at $\theta_r = 0°$, the spins evolve under $H$ (Eq. (5)) for a time $t$. $H$ can be generated by sandwiching $H_D^{HF}$ between two 90°Y pulses, with an additional $\pi$ pulse at $t/2$ in order to refocus CSA, giving $k = 1$. Then to generate $H^{EVO}$ the above sequence of $\delta$–pulses is applied after the rotor has been mechanically flipped to $\theta_r = 90°$. In the limit $N \to \infty$, $g = \frac{3}{8}$. In order to cancel the $\theta$ dependence, the evolution times must satisfy the condition:

$$t = \frac{2}{3}g\tau. \quad (19)$$

Using $g = \frac{3}{8}$ gives $\tau = 4t$, and gives a dipolar scaling factor, $\sigma$, of:

$$\begin{aligned} \sigma\omega_D &= \frac{\omega_D}{t+\tau}\left(\frac{3}{4}t\left(3\cos^2(\theta) - 1\right) + \frac{3}{2}g\tau\sin^2(\theta)\right) \\ &= \frac{3\omega_D}{10}. \end{aligned} \quad (20)$$

This methodology does not require repeated switching back and forth between the two rotor angles since it is not the Hamiltonians but the frequencies which are combined in order to get isotropic dipolar spectra. The spectrum contains two peaks with splitting of $\omega = \pm 0.3\omega_D$, which is the predicted maximum splitting obtained by reconstructing the zero-field Hamiltonian, $H_D^{ZF}$, from the truncated dipole Hamiltonian [8]. Since the limit $N \to \infty$ is not realistic, a finite $N$ must be chosen. For $N = 8$, the maximum scaling for $H^{EVO}$ is $g = 0.337$, giving $\tau = 4.44t$ and $\sigma = 0.28$. In the absence of CSA, the resulting spectrum is shown in Fig. 3b. However, in the presence of CSA, the sequence does not perform nearly as well (Fig. 3c). Better methods are therefore required in order to compensate for CSA and offsets effects during the sequence.

The post-C$N_n^v$ sequences [17], which are offset and RF-inhomogeneity compensated variants of the C$N_n^v$ sequences [18], contain continuous irradiation, rotor-synchronized pulses. The post-C$N_n^v$ consists of $N$, phase-incremented blocks over a period of $n$ rotor cycles, where the $k$th block is given by $[(\pi/2)_0(2\pi)_\pi(3\pi/2)_0]_{\phi_k}$, where $\phi_k = 2\pi v/N$. The pulse sequence post-C$N_2^0$ can be used to generate $H$ (Eq. (5)). This gives a scaling factor $k$ of

$$\begin{aligned} k &= -\frac{1}{2}\left(\frac{3\cos^2(\theta_r) - 1}{2}\right) \\ &= \bar{k}\left(\frac{3\cos^2(\theta_r) - 1}{2}\right). \end{aligned} \quad (21)$$

The pulse sequence post-C$N_2^2$ can be used to create $H^{EVO}$ since it generates terms like $A_{2,\pm 2}T_{2,\mp 2}$ in the Hamiltonian. However, unwanted terms like $A_{2,\pm 1}T_{2,\mp 1}$ and $A_{2,\pm 1}I_\mp$ are also generated. These

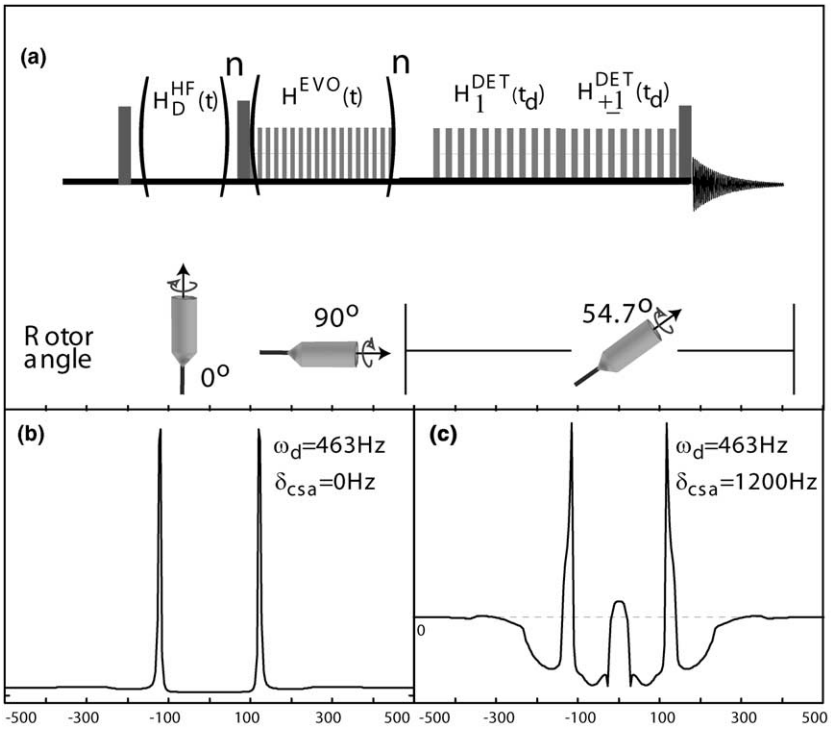


Fig. 3. (a) An ideal sequence that gives the maximum scaling factor, $\sigma = 0.3$. The spins evolve under $H$ for a time $t$, with $k = 1$ in Eq. (5) while spinning the rotor at $\theta_r = 0°$. Next the rotor is flipped to $\theta_r = 90°$, and the spins evolve under $H^{EVO}$ for a time $\tau$ which, as discussed in the text, can be generated with a maximum $g$ of 3/8. Next the rotor is then flipped to the magic angle, and $H^{DET}$ is then applied. (b) Simulation [20] of the above sequence for a pair of dipole coupled spins with $\omega_D/(2\pi) = 463$ Hz, $\omega_{CSA}/(2\pi) = 0$ Hz, and $\omega_r/(2\pi) = 5$ kHz. $\tau = 4.44$ t was used (as described in the text), giving $\sigma = 0.28$. An RF field strength of 150 kHz was used. (c) Same experiment as in (b) but with $\omega_{CSA} = 1200$ Hz. Notice the deterioration of the isotropic spectrum.

unwanted terms can be removed by applying another cycle of post-C$N_2^2$ but with an additional $\pi$ phase shift. The factor, $g$, for the $(\text{post-C}N_2^2)_0 - (\text{post-C}N_2^2)_\pi$ becomes

$$g = \frac{3\sin(\frac{4\pi}{N})N^3\sin^2(\theta_r)}{64\pi(N^2-1)} = \bar{g}\sin^2(\theta_r), \tag{22}$$

Finally, the detection Hamiltonian, $H_{\pm 1}^{DET}$, can be created by using the post-C$7_2^{\pm 1}$ sequence [17], with the only requirement being that the sample is not spinning at either $\theta_r = 0°$ or $\theta_r = 90°$, due to the fact that the scaling factor, $f$, from Eq. (11) is zero under these conditions. Evolution under $H^{DET}$ only affects the intensities of the resulting signal (Eq. (14)), but not $\sigma$.

The requirement of spinning the sample about different axes during the course of the experiment, while leading to a larger $\sigma$, can be experimentally demanding. However, the above methodology can also be applied to samples spinning about only one rotor axis. Under this condition, the evolution must satisfy

$$\left|\frac{\omega_D}{t+\tau}\left(\frac{3}{2}\bar{k}t\frac{(3\cos^2(\theta_r)-1)}{2}\frac{(3\cos^2(\theta)-1)}{2} \pm \frac{3}{2}\bar{g}\tau\sin^2(\theta_r)\sin^2(\theta)\right)\right| = \left|\frac{3k\omega_D t}{2(t+\tau)}\right|. \tag{23}$$

When $\theta_r \neq 0°$, t and $\tau$ must typically be multiples of the rotor period. From Eq. (23), the rotor angle ($\theta_r$) that the sample must be spun at is given by

$$\theta_r = \arccos\left(\sqrt{\frac{3\bar{k}t \pm 4\bar{g}\tau}{9\bar{k}t \pm 4\bar{g}\tau}}\right). \quad (24)$$

Note that by spinning along one axis, $\theta_r = 0°$ and $\theta_r = 54.7°$ are excluded as solutions to Eq. (24). In addition, $\theta_r = 90°$ is excluded on the grounds that $H_{\pm 1}^{DET}$ is zero under this condition.

## 4. Experimental

Experiments were performed on a Chemagnetics (now Varian, Palo Alto, CA) spectrometer with a 4.2 T magnet (180 MHz $^1$H). The sample used was $^{13}C_2$-methyl dimethyl malonic acid (DMMA) diluted to 30% in natural abundance dimethyl malonic acid and was provided by Herbert Zimmermann. The sample was spun at 5 kHz in a 4 mm HX Chemagnetics probe. The spinning angle was set manually. Following a ramped cross polarization period, proton decoupling of 150 kHz was used during the indirect evolution as well as in the directly detected dimension. Eighty $t_1$ points were collected in the indirect dimension with a dwell of 1.2 ms.

## 5. Results and discussion

The experiment in Fig. 4 was performed in order to obtain an isotropic dipolar spectrum. $H$ was created by applying the sequence post-$C7_2^0$, with a corresponding scaling factor of $\bar{k} = -1/2$ (Eq. (21)). $H^{EVO}$ was created using a (post-$C7_2^2$)$_0$–(post-$C7_2^2$)$_\pi$ sequence, with a corresponding scaling factor of $\bar{g} = 0.104$ (Eq. (22)). Sixteen cycles of $H_{\pm}^{DET}$ were used, allowing theoretically $C = 0.23$ amount of the total magnetization to be converted

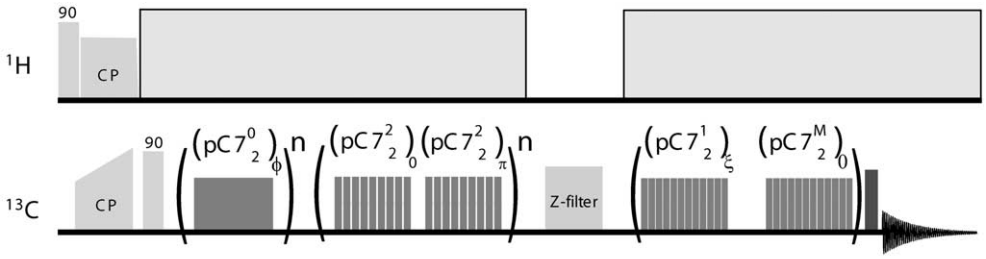


| experiment | ϕ (deg) | ξ (deg) | M | receiver phase |
|---|---|---|---|---|
| $X_1$ | 0 | 0 | 1 | -1 |
| $X_2$ | 0 | 90 | 1 | 1 |
| $Y_1$ | 90 | 0 | 1 | -1 |
| $Y_2$ | 90 | 90 | 1 | 1 |
| 2 *$X_3$ | 0 | 0 | -1 | 1 |
| 2 *$X_4$ | 0 | 90 | -1 | -1 |
| 2 *$Y_3$ | 90 | 0 | -1 | -1 |
| 2 *$Y_4$ | 90 | 90 | -1 | 1 |

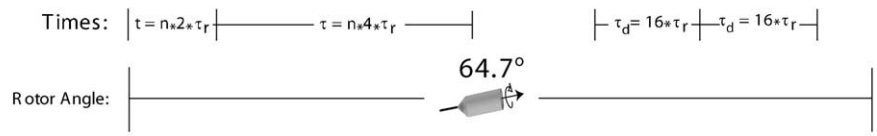


Fig. 4. Actual experiments performed in order to obtain isotropic dipolar spectra. The pulse sequence along with the corresponding phase cycle is presented. The first four experiments correspond to evolution from $\rho_0$ in Fig. 2. The last four experiments correspond to evolution from $\rho_2$ in Fig. 2. The last four experiments have to be performed twice as required from Eq. (14).

into signal (Eq. (16)). Experimentally, $\approx 16\%$ of the magnetization was converted into signal. With the condition $\tau = 2t$, Eq. (24) gives a rotor axis of $\theta_r = 64.7°$, and Eq. (23) gives a scaling factor of $\sigma = -0.0566$. Fig. 5 shows the experimental and simulated spectra. The spectrum consists of two peaks at $\pm(26.3 \pm 3.3)$ Hz. Using the scaling factor $\sigma = -0.0566$ results in an estimated distance between the two $^{13}C$ nuclei of $2.54 \pm 0.16$ Å, which is in good agreement with the previously reported distance [19] of 2.541 Å. Angle missettings, pulse imperfections, and higher-order terms in the average Hamiltonians could all contribute to deviations from the predicted behavior.

Homonuclear isotropic evolution works by refocusing the anisotropic contributions of the dipolar interaction by generating a series of various Hamiltonians whose frequencies can be used to cancel the anisotropic terms. Although the experimental scaling of the dipolar couplings was roughly a factor of two lower than the experimentally observed scalings for the previous ZFHF experiments, it was shown that both methods give the same theoretical maximum scaling of $\sigma = 0.3$. Larger scaling factors can be obtained by spinning the sample at multiple angles as discussed earlier. Since the refocusing of the anisotropy comes from combining the frequencies and not the Hamiltonians, the sample does not have to be repeatedly switched between different angles, which is experimentally feasible but still difficult. The ability to switch between multiple spinning angles would be useful in correlating the isotropic dipolar spectra to the magic-angle spinning isotropic chemical shift spectra, which can be done by applying $H^{DET}$ at the magic-angle as shown in Fig. 3.

There are several limitations that the HOMIE method has that the ZFHF does not. First of all, HOMIE only works for pairs of homonuclear coupled spins, whereas ZFHF constructs the zero-field Hamiltonian for any number of spins. Although it may be possible to extend HOMIE to higher number of spins, HOMIE would only be useful in samples of randomly labeled spin pairs. Secondly, only a fraction of the magnetization, $C$ (Eq. (16)) is used in the HOMIE experiment, whereas all the magnetization is potentially used in the ZFHF experiment.

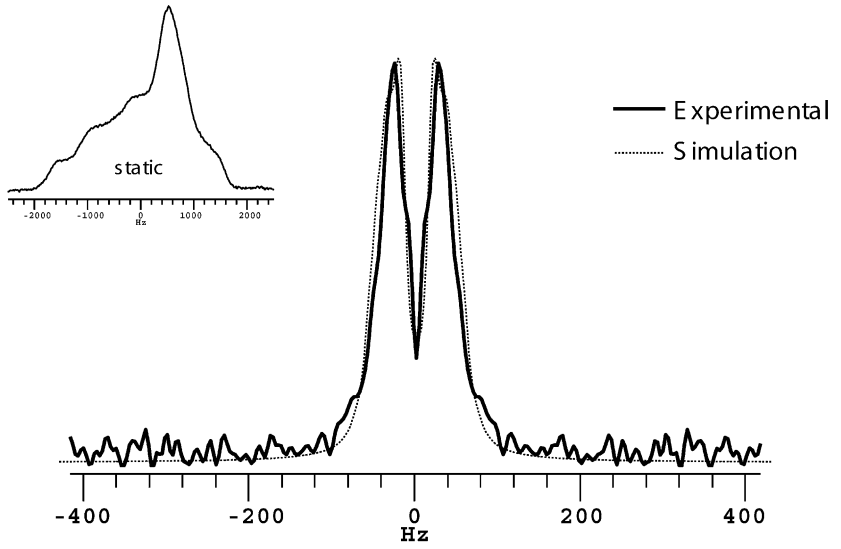


Fig. 5. Simulation [20] (dashed line) and experimental (solid line) data of the sequence shown in Fig. 4 on $^{13}C_2$-methyl dimethyl malonic acid (DMMA). Simulation attempted to model DMMA with $\omega_D/2\pi = 463$ Hz, $\omega_{CSA}/2\pi = 1200$ Hz, while spinning at 5 KHz. A 10 Hz line broadening was added to the simulation to match the experiment as best as possible. Both the simulated and the experimental spectra give a good match to the scaling factor of $\sigma = 0.0566$. The small spectrum in the left hand corner is the static experimental spectrum of DMMA.

The biggest advantage of this methodology would be in its potential application to isotropic proton detected local field spectroscopy. Consider a system of $N$ protons, homonuclear decoupled from one another, that are dipole coupled to a $^{13}C$ nucleus. At high-field, observing the proton signals under the heteronuclear dipolar Hamiltonian would result in $N$ overlapping heteronuclear Pake patterns. Due to the limited chemical shift range of the protons, deconvolving the Pake patterns could prove to be very difficult. The anisotropic broadening could be removed by creating the zero-field heteronuclear Hamiltonian using a method similar to Tycko's ZFHF technique. However, the zero-field heteronuclear dipolar Hamiltonian of different protons typically do not commute; this leads to a complicated spectrum with structural information not easily ascertained. However, the methodology presented in this Letter could potentially be used instead since it involves only combining frequencies and not Hamiltonians in order to refocus the anisotropy. The resulting spectrum would consist of $N$ isotropic doublets, with the splitting proportional to the heteronuclear dipolar coupling. Experiments are currently underway in our group along this direction.

## Acknowledgements

We would like to thank Herbert Zimmermann for providing us with the DMMA sample used in our experiments. R.H.H. acknowledges the National Science Foundation for a predoctoral fellowship. This work was supported by the Director, Office of Science, Office of Basic Energy Sciences, Materials Science and Engineering Division, US Department of Energy under Contract No. DE-AC03-76SF00098.

## References

[1] M. Salzmann, K. Pervushin, G. Wider, H. Senn, K. Wuthrich, J. Am. Chem. Soc. 122 (2000) 7543.
[2] D. Wemmer, Method Enzymol. 309 (1999) 536.
[3] D. Laws, H. Bitter, K. Liu, H. Ball, K. Kaneko, H. Wille, F. Cohen, S. Prusiner, A. Pines, D. Wemmer, Proc. Natl. Acad. Sci. USA 98 (2001) 11686.
[4] J. van Beek, L. Beaulieu, H. Schafer, M. Demura, T. Asakura, B. Meier, Nature 405 (2000) 1077.
[5] J. Klinowski, Anal. Chim. Acta 283 (1993) 929.
[6] J. Griffiths, R. Griffin, Anal. Chim. Acta 283 (1993) 1081.
[7] D. Weitekamp, A. Bielecki, D. Zax, K. Zilm, A. Pines, Phys. Rev. Lett. 50 (1983) 1807.
[8] R. Tycko, J. Magn. Reson. 75 (1987) 193.
[9] R. Tycko, Phys. Rev. Lett. 60 (1988) 2734.
[10] R. Tycko, J. Chem. Phys. 92 (1990) 5776.
[11] U. Haeberlen, J. Waugh, Phys. Rev. 175 (1968) 453.
[12] R. Tycko, G. Dabbagh, J. Duchamp, K. Zilm, J. Magn. Reson. 89 (1990) 205.
[13] B.Q. Sun, A. Pines, J. Magn. Reson. A 109 (1994) 157.
[14] B. Chmelka, K. Mueller, A. Pines, J. Stebbins, Y. Wu, J. Zwanziger, Nature 339 (1989) 42.
[15] A. Llor, J. Virlet, Chem. Phys. Lett. 152 (1988) 248.
[16] A. Samoson, E. Lippmaa, A. Pines, Mol. Phys. 65 (1988) 1013.
[17] M. Hohwy, H.J. Jakobsen, M. Eden, M.H. Levitt, N.C. Nielsen, J. Chem. Phys. 108 (1998) 2686.
[18] Y.K. Lee, N.D. Kumur, M. Helmle, O.G. Johannessen, N.C. Nielsen, M.H. Levitt, Chem. Phys. Lett. 242 (1995) 304.
[19] H. Sheng-Zhi, T. Mak, Acta Crystallogr., Sect. C (Cr. Str. Comm.) 42 (1986) 1456, CSD ref. MMALAC01.
[20] W. Blanton, Blochlib: a fast, object-oriented, nmr and bloch equation c++ library. Manuscript in preparation, look to http://waugh.cchem.berkeley.edu/blochlib/ for more information.